The Rocket Experiment Demonstration of a Soft X-ray Polarimeter (REDSoX Polarimeter)

Herman L. Marshall[a], Norbert S. Schulz[a], Sarah N. Trowbridge Heine[a], Ralf K. Heilmann[a], H. Moritz Günther[a], Mark Egan[a], Tim Hellickson[a], Mark Schattenburg[a], Deepto Chakrabarty[a], David L. Windt[b], Eric M. Gullikson[c], Brian Ramsey[d], Martin C. Weisskopf[d], Gianpiero Tagliaferri[e], Giovanni Pareschi[e], Alan Marscher[f], Svetlana Jorstad[f]

[a]MIT Kavli Institute, Cambridge, MA, USA 02139
[b]Reflective X-ray Optics, 1361 Amsterdam Ave, Suite 3B, New York, NY, USA 10027
[c]Lawrence Berkeley National Lab, 1 Cyclotron Rd., Bldg. 2R0400, Berkeley, CA, USA 94720
[d]NASA Marshall Space Flight Center, Huntsville, AL, USA
[e]Istituto Nazionale di Astrofisica, Brera, IT
[f]Boston University, Boston, MA

ABSTRACT

The Rocket Experiment Demonstration of a Soft X-ray Polarimeter (REDSoX Polarimeter) is a sounding rocket instrument that can make the first measurement of the linear X-ray polarization of an extragalactic source in the 0.2-0.8 keV band as low as 10%. We employ multilayer-coated mirrors as Bragg reflectors at the Brewster angle. By matching the dispersion of a spectrometer using replicated optics from MSFC and critical angle transmission gratings from MIT to three laterally graded multilayer mirrors (LGMLs), we achieve polarization modulation factors over 90%. We present a novel arrangement of gratings, designed optimally for the purpose of polarimetry with a converging beam. The entrance aperture is divided into six equal sectors; pairs of blazed gratings from opposite sectors are oriented to disperse to the same LGML. The LGML position angles are 120 degrees to each other. CCD detectors then measure the intensities of the dispersed spectra after reflection and polarizing by the LGMLs, giving the three Stokes parameters needed to determine a source's linear polarization fraction and orientation.

A current grant is funding further development to improve the LGMLs. Sample gratings for the project have been fabricated at MIT and the development team continues to improve them under separate funding. Our technological approach is the basis for a possible orbital mission.

Keywords: X-ray, polarimeter, astronomy, multilayer, mirror, grating

1. INTRODUCTION

We have developed a robust design for a soft X-ray polarimeter based on Bragg reflection from multilayer-coated optics. Marshall (2007[1]) described the basic method, using transmission gratings to disperse the incoming X-rays so that the dispersion is matched to laterally graded multilayer coated mirrors (LGMLs). Here, we describe a design of the proposed instrument, leaving details of the engineering design and raytrace verification to companion papers [2, 3]. The experiment's minimum detectable polarization (MDP) is expected to be better than 11% when observing a bright blazar such as Mk 421, which we expect to be polarized in the soft X-ray band at about the 20% level. For isolated, highly magnetized neutron stars, the instrument should detect the effects of vacuum birefringence.

Associated laboratory work has demonstrated many of the design details. We have tested LGMLs that give reflectivities better than 10% in the 45-75 Å band [4]. Critical angle transmission (CAT) gratings have been made and tested that achieve efficiencies over 20% [5]. We have been testing various aspects of CAT gratings in the MIT Polarimetry lab [6].

Further author information: (Send correspondence to H.L.M.)
H.L.M.: hermanm@space.mit.edu, Telephone: 1 617 253 8573

UV, X-Ray, and Gamma-Ray Space Instrumentation for Astronomy XX, edited by Oswald H. Siegmund,
Proc. of SPIE Vol. 10397, 103970K · © 2017 SPIE · CCC code: 0277-786X/17/$18 · doi: 10.1117/12.2274107

Figure 1. Cutaway rendering of the *REDSoX* Polarimeter from engineering design, showing the optics at left, gratings (in gold), the optical bench, the focal plane baffle (with three slits for dispersed events) over the pendulum valve for the detector chamber, and the back of the detector chamber with the electronics box. The top and bottom grating groups intercept opposite 60° sectors of focused X-rays, dispersing them through the baffle slit to the left of the central (rectangular) aperture for 0th order. For clarity, only a few mirror shells and grating groups are rendered.

2. SCIENCE OBJECTIVES

2.1 Overview

The scientific goal of the Rocket Experiment Demonstration of a Soft X-ray Polarimeter (the *REDSoX* Polarimeter, Fig. 1) is to make the first measurement of linear X-ray polarization below 1 keV. The value of X-ray polarimetry to the scientific community was underscored by NASA's selection of the Imaging X-ray Polarimetry Explorer (IXPE, [7]), the most recent NASA SMEX cycle. IXPE uses photoelectron-tracking detectors with sensitivity only above 2 keV, while the *REDSoX* Polarimeter provides complementary capability that is a step in a development path toward an orbital mission, which is our technical goal.

Some sources, such as many isolated neutron stars (NSs) are only detectable below 1 keV. Our design [8] provides a broad-band capability for this energy range. We have been developing the technology for soft X-ray polarimetry under the NASA Astrophysics Research and Analysis (APRA) program and now believe that our soft X-ray polarimeter design is ready for a flight demonstration on a sounding rocket. Our baseline design relies on components whose performances have been verified. Our first target is a bright, jet-dominated BL Lac object to test models of jet B-field geometry on small scales. Our second target will be an isolated NS to test predictions of quantum electrodynamics in a strong magnetic field.

2.2 Scientific Value of Soft X-ray Polarimetry

As the prospects for measuring X-ray polarization have improved over the past decade, there is now significant theoretical work bolstering the need for X-ray polarimeters. Here we describe potential scientific studies to be performed with an X-ray polarimetry mission with sensitivity in the 0.1-0.7 keV band that would not be covered by instruments such as IXPE. We include a discussion of additional science goals that would be attainable, either in later flights or with an orbital version of the *REDSoX* Polarimeter (see § 4).

2.2.1 Probing the Relativistic Jets in BL Lac Objects

Blazars, which include BL Lac objects, high polarization quasars, and optically violent variables, contain parsec-scale jets with $\beta \equiv v/c \sim 0.995$ or higher. In the so-called high-synchrotron-peak blazars (HBLs such as Mk 421 & Mk 501), the X-ray spectrum is steeper than the optical spectrum, indicating that the X-rays are produced by synchrotron radiation from the highest energy electrons that are efficiently accelerated close to the base of the jet or at shock fronts farther downstream in the jet. For a differential electron energy distribution $n(E) \propto E^{-p}$, the maximum fractional polarization for synchrotron emission from relativistic electrons in a uniform B field is $P_{\rm max} = \frac{p+1}{p+7/3}$ [9]. The spectral shape is a power law with energy index $\alpha = (p-1)/2$, so the photon index is $\Gamma = (p+1)/2$ and $P_{\rm max} = \Gamma/(\Gamma + 2/3)$. For Mk 421, Γ is typically about 2.5 in the soft X-ray band, giving $P_{\rm max} = 0.79$, i.e., 79% polarized.

In the optical band, where $\Gamma \sim 1.5$, $P_{\rm max}$ is calculated to be about 70% but observed optical polarization fractions (after subtraction of the host galaxy emission) range only up to $\sim$ 30% [10, 11, and Jorstad et al. in prep.], so models in which the jet plasma is turbulent have been developed to account for the observed

polarization fraction. In an approximation where the emitting plasma is divided into $\mathcal{N}$ cells, each with a uniform but randomly directed magnetic field, the mean degree of linear polarization is $\langle P \rangle = P_{\rm max}\mathcal{N}^{-1/2}$ [12]. A median optical polarization of 10% would correspond to $\mathcal{N}_{\rm opt} \sim 50$. $\mathcal{N}$ could be even higher if shock compression partially orders the turbulent field as the plasma crosses a shock in the jet, in which case P can range up to $\sim 40\%$, depending on the viewing angle and the compression ratio of the shock.

Jet and shock models make different predictions regarding the direction of the magnetic field at X-ray energies. For knots in a laminar jet flow with cross-jet velocity gradients (as found in Mk 501 [13]), the magnetic field can be nearly parallel to the jet axis [14], while for internal shocks it should be perpendicular [15]. Turbulence causes both the degree and position angle of the polarization to vary erratically about any systematic values. In the shock model, the emitting volume decreases with frequency as $\nu^{-1/2}$ because of energy losses of the emitting electrons as they advect from the shock front where they are energized. This decreases the number of emitting turbulent cells at higher frequencies, $\mathcal{N} \propto \nu^{-1/2}$. This model therefore predicts an X-ray polarization at 0.3 keV that is 3.7 times the optical R-band value, giving expected polarizations of about 20% and 40% for Mk 421 and Mk 501, respectively. Measurement of both the X-ray and optical polarization therefore has the potential to decide among the different scenarios for explaining the highly efficient particle acceleration in HBLs.

The most puzzling aspect of Mk 421, Mk 501, and other TeV-bright BL Lac objects is the extremely short time-scale of some pronounced flux variations at X-ray and TeV energies, which can be as short as 15 min [e.g. 16]. This could result from the highest energy emission arising from very close to the black hole. Alternatively, a small fraction of the jet on parsec scales could receive a sudden infusion of electrons with energies up to $\sim 10^5\ m_e c^2$. Of all the lower-frequency bands, the X-ray flux is most closely correlated with TeV γ-rays, hence measurement of the X-ray polarization is among the few methods that can probe the physical conditions in the TeV-emitting plasma of blazar jets, where particle acceleration is dramatically impulsive and efficient.

Both Mk 421 and Mk 501 are highly variable HBLs. Mk 421 is brighter at present, so it is our primary target. To estimate the expected brightness, we take the median count rate of Mk 421 from the Swift XRT over the past 10 years as a baseline: 28.5 cnt/s. About 20% of the time, the count rate is $\times 2$ higher. Converting to a spectral flux density using $\Gamma = 2.5$ gives 0.030 ph cm^{-2} s^{-1} Å^{-1} at 0.3 keV. For the *REDSoX* Polarimeter, the expected minimum detectable polarization (MDP) is 11% (see § 3.3.4), which is sufficient for our scientific goal. Mk 501, as an alternative, is fainter but the predicted polarization is higher. A decision about which target to observe can be made closer to launch, based on monitoring observations (as ongoing with Swift), with the key criterion being the lowest possible MDP.

2.2.2 Isolated Neutron Stars and Pulsars

Isolated neutron stars (NSs) with strong magnetic fields are often very soft; they are too faint above 2 keV for IXPE but excellent targets for the *REDSoX* Polarimeter. For photons propagating perpendicular to the local B, the surface emission is expected to show a net polarization due to asymmetric opacities for the two normal modes (where the E-vector is either parallel or orthogonal to the local B). The pattern across the surface and variation with rotational phase depend on the atmosphere [17, 18], so a polarimeter can diagnose the surface conditions. An example is shown in Fig. 2 (left) where spectral features are clearly polarized.

Interestingly, when B is comparable to the quantum critical magnetic field, where the electron's cyclotron energy equals its rest mass (at $B_c = m_e^2 c^3/e\hbar = 4.4 \times 10^{13}$ G) then the X-ray polarization can be profoundly affected by quantum electrodynamics (QED) effects. Vacuum birefringence, or vacuum polarization [19, 20, and references therein], arises as the indices of refraction for linearly polarized light change in a strong magnetic field [21]. The extent of polarized radiation from the surface of a neutron star increases up to 100% when QED propagation effects are included in the calculation [19]. Photons with E-vectors orthogonal to the magnetic field are converted to photons with parallel E-vectors. The effect is small until the photon propagates through a distance sufficient to rotate the E-vector into local alignment, $\sim 10^7$ cm, after which the photons' polarization directions are frozen. Fig. 2 shows an illustration of how QED affects the initially randomly polarized emission from the surface. Our primary target for such an observation is RX J1856.4−3754, the brightest isolated NS in the ROSAT all sky catalog. A birefringence model of this source gave a prediction in the soft X-ray band of $\gtrsim 90\%$ polarization [22], validated by an optical polarization detection of 16% [23]. The MDP for the *REDSoX* Polarimeter is 59%, sufficient to test the model.

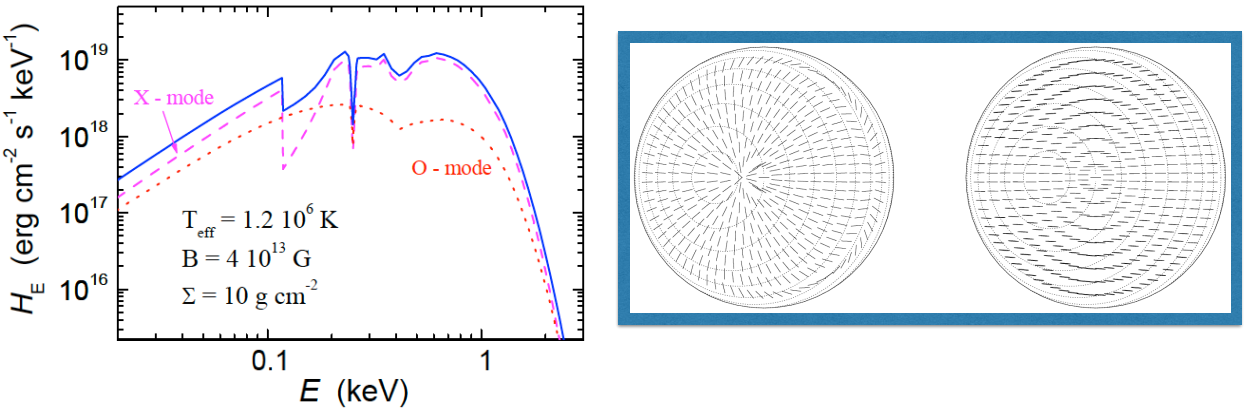

Figure 2. *Left:* Model spectra giving the total spectrum (blue) and the polarized spectra (magenta and red) for a neutron star atmosphere [18]. The absorption edges show up primarily in X-mode radiation, where the E-vector is perpendicular to the local B-field direction, as these photons originate deeper in the stellar atmosphere. *Right:* Polarization vectors on the apparent surface of a strongly magnetized neutron star with (right) and without (left) the effect of vacuum birefringence expected in quantum electrodynamics (QED) [19]. Concentric circles indicate lines of magnetic latitude. Without this QED effect, polarization directions across the surface vary considerably, showing no net polarization. In QED, the photons are polarized according to the well ordered field far from the surface, resulting in nearly 100% polarization.

A broad absorption line at 0.3 keV in the soft X-ray spectrum of RX J0720.4−3125 is consistent with a proton cyclotron line [24]. If so, the isolated NS may be a "magnetar" with $B \gtrsim B_c$. Such isolated NSs are thought to be powered by the decay of enormous magnetic fields. Haberl (2007 [25]) pointed out in a review that there are several isolated NSs known to have absorption features in the soft X-ray band. Suleimanov (2010 [18]) predicted that absorption in soft X-ray spectra will be differently polarized than the nearby continuum, so spectropolarimetry could test the nature of these absorption features (see Fig. 2). RX J0720 is an alternate target to RX J1856 because it is slightly fainter; the MDP attainable by the *REDSoX* Polarimeter would be just under 75%. PSR B0656+14, a radio pulsar, is similarly X-ray bright and visible from the northern hemisphere. Her X-1, an accreting pulsar in a binary with an A star is another interesting target. The 50% pulsed soft X-ray emission could be nearly 100% polarized according to one model [26] or it could be more like 10-20% (Caiazzo & Heyl, in prep.). It is bright and has low N_H. We expect MDP = 20% using the *REDSoX* Polarimeter, so these two models could be readily distinguished in an observation during a high state in its 35 day cycle.

Because there are several good targets for the *REDSoX* Polarimeter, our observing strategy is flexible. The prime target for our second launch is RX J1856, which requires a launch from Australia. If the time of year for such launches is bad for this target, then RX J0720 can be chosen instead. If only US launches are available, then PSR B0656 is the prime candidate unless the time of year is bad for it, in which case we choose Her X-1 as the target. All are candidates for later flights, especially with instrument upgrades.

2.2.3 Polarization in Disks and Jets of Active Galaxies and X-ray Binaries

Other targets for the *REDSoX* Polarimeter, or an orbiting version of it, are quasars and X-ray binaries (XRBs). X-ray emission from accretion onto black holes may arise from Compton scattering of thermal photons in a hot corona or from synchrotron emission or Comptonization by electrons in a highly relativistic pc-scale jet. Jets are frequently observed from such sources, so the X-rays should be polarized. In both cases, the origin of the jet is not resolved in the X-ray band, so X-ray polarization measurements can give an indication of the existence and orientation of jets within 10^3 gravitational radii.

Transient XRBs with stellar-mass black holes like XTE J1118+480 can be very soft and jets may contribute most of the X-rays [27] – confirmable using polarimetry. A jet model for XTE J1118 indicates that the soft X-ray polarization should be about 20% [28]. The source was discovered with XTE and detected by the Extreme Ultraviolet Explorer at 100 eV, so the column density is well below 10^{20} cm^{-2}, making it a good target for the *REDSoX* Polarimeter. During its 2000 outburst, the flux density at 0.3 keV was brighter than Mk 421 [29], making it an excellent candidate for a target of opportunity for the *REDSoX* Polarimeter, should it, or an XRB like it, go into outburst after instrument integration.

Theoretical work indicates that AGN accretion disks and jets should be 10-20% polarized [30, 31] and that the polarization angle and magnitude should change with energy in a way that depends on the system inclination.

The variation of polarization with energy could be used as a probe of the black hole spin and the polarization position angle should rotate through 90° between 1 and 2 keV [31]. Thus X-ray polarization measurements are needed both above 2 keV (with IXPE, for example) and below 1 keV with an orbital mission based on the *REDSoX* Polarimeter (see § 4).

3. TECHNICAL APPROACH

3.1 Overview

The science payload consists of the X-ray optics with Wolter type I mirror shells, 200 nm period Critical Angle Transmission (CAT) gratings mounted on a 2.5 meter focal length optical bench, the focal plane with its four X-ray detectors and three multi-layer mirrors in a high vacuum chamber that is open only while the instrument is over 120 km altitude. See Fig. 1 for an engineering rendering and Fig. 3 for raytrace illustrations of operation.

The basic design involves matching the dispersion of the gratings to the lateral grading of a multilayer (ML) coated mirror set at about 45° to the incoming light. In the X-ray band, this orientation nulls the reflectivity of the polarization in the plane of the reflection; the reflected light is 100% polarized with the electric vector perpendicular to the reflection plane. CCD detectors view each ML mirror to determine the intensity reflected from that ML mirror. By orienting three ML coated mirrors at position angles 120° apart, we can measure three Stokes parameters (I, Q, and U) at any time without instrument rotation. The fraction of polarized light is given by $\Pi = \sqrt{Q^2 + U^2}/I$. The 0th order CCD detector also can be used to determine I, providing some redundancy.

We now describe the components of the *REDSoX* Polarimeter in its baseline configuration. All components have been demonstrated in flight projects (§ 3.2.1), in our polarimetry beamline [6], or are in development for approved flight projects (§ 3.2.4). Engineering details are left to a companion paper (Egan et al., this volume).

3.2 Baseline Components

3.2.1 Focussing Optics

The polarimeter optics proposed here will be fabricated using an electroformed replication process. In this process, nickel alloy mirror shells are electroformed on super-polished and figured aluminum mandrels from which they are later separated. The resulting full-shell optics are stable, durable, and have good angular resolution [32].

For this project, we take advantage of mandrels fabricated at the Marshall Space Flight Center (MSFC) for the Micro-X sounding rocket program [33]. One mandrel is shown in Fig. 4 (left). For the *REDSoX* Polarimeter, a 9-shell mirror module is basedlined. Each shell will follow a Wolter-1 prescription with a total length (paraboloid + hyperboloid) of 600 mm and a thickness of 1 mm. Accounting for 12% obscuration by mounting structures and the reflectivity of Ni at 1.0-1.3° graze angles, the optics module will provide an effective area of 457 cm^2. MSFC will cooperate on the optics fabrication task with the Brera Astronomical Observatory (part of INAF, the Italian Institute for astrophysics) and Media Lario.

The focal length is 2500 mm, giving a focal plane scale of $82''$/mm. The mirror module will have a half-power diameter (HPD) of $\lesssim 30''$ [32]. As with other grating spectrometer designs, we will subaperture the mirror (Figs. 4 and 5), placing grating modules behind $\pm 30°$ sectors on opposite sides of the focussing light path to reduce the telescope 2D PSF from $30''$ to $10''$ in 1D (see Fig. 9) for use in spectroscopy [34], projecting to $\delta x = 120\mu$m along the dispersion. To match the spectral bandpass of the LGML, the grating spectrometer should have a resolving power $R = E/\delta E > 100$, because the multilayers have Bragg reflectivity peaks that are $\delta E/E = 0.020$ to 0.025 wide (FWHM). For a grating spectrometer, $R = \lambda/(\delta\lambda) = x/(\delta x)$; $x = 24 - 56$ mm is the dispersion distance for the gratings in our design (§ 3.2.2) and the baseline wavelength range of 30-70 Å. At these dispersion distances, R is in the range 200 to 467, at least $\times 2$ better than the requirement.

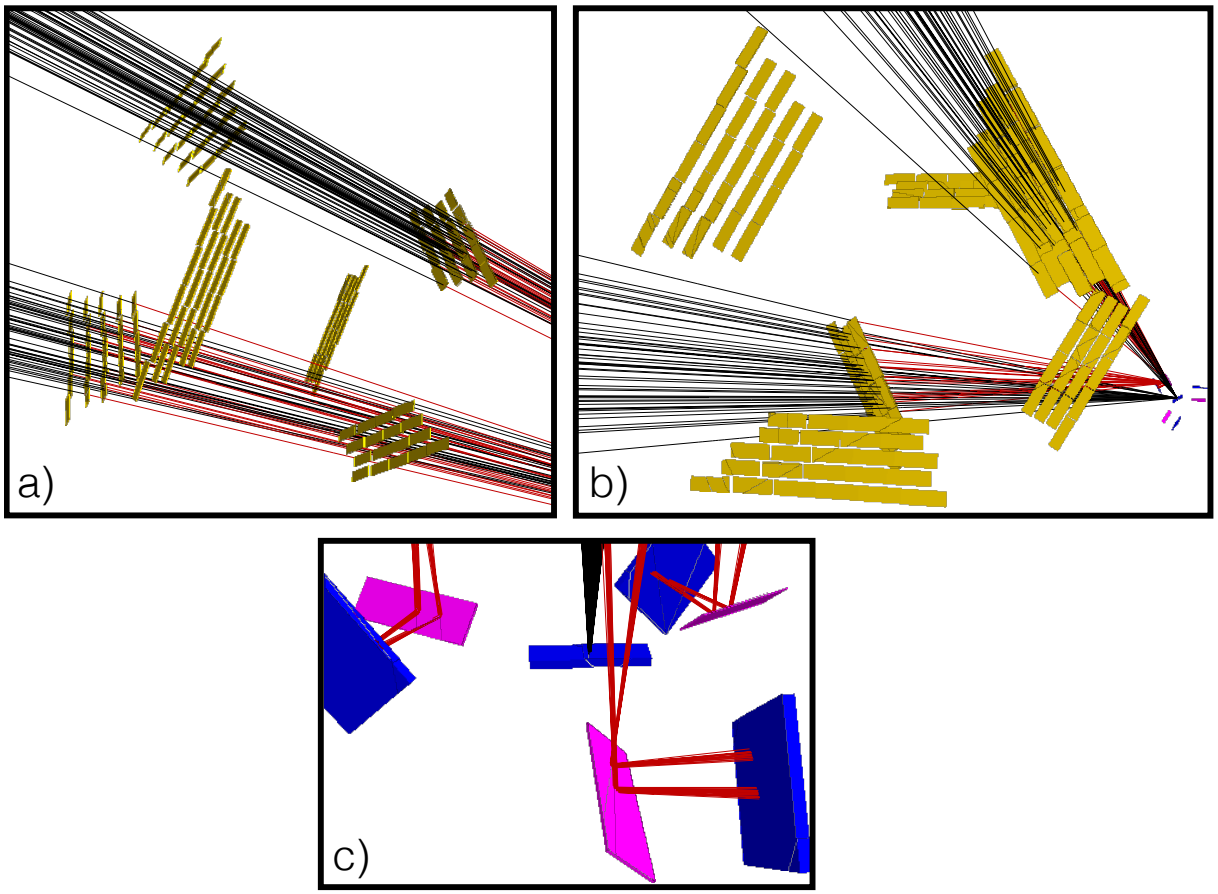

Figure 3. Raytrace views of the *REDSoX* Polarimeter. *a)* and *b)* The focusing optics are to the upper left and its output rays are black lines. Rays of $E = 0.25$ keV going through only two opposing 60° sectors are shown; rays dispersed by the gratings (in gold) are colored red. Grating groups are paired, with an upper group closer to the optics and a lower group closer to the focal plane. In *b)*, the view is foreshortened to include the focal plane. *c)* Rays dispersed by the gratings (red) hit the laterally graded multilayer mirrors (LGMLs, magenta) before arriving at corresponding CCDs (blue). Photons coming from the upper and lower grating groups in opposing sectors arrive at different positions along an LGML, where the Bragg condition is satisfied for rays incident at angles differing from 45° (see § 3.2.2 for details). Black lines represent 0th order photons going to the direct imaging CCD.

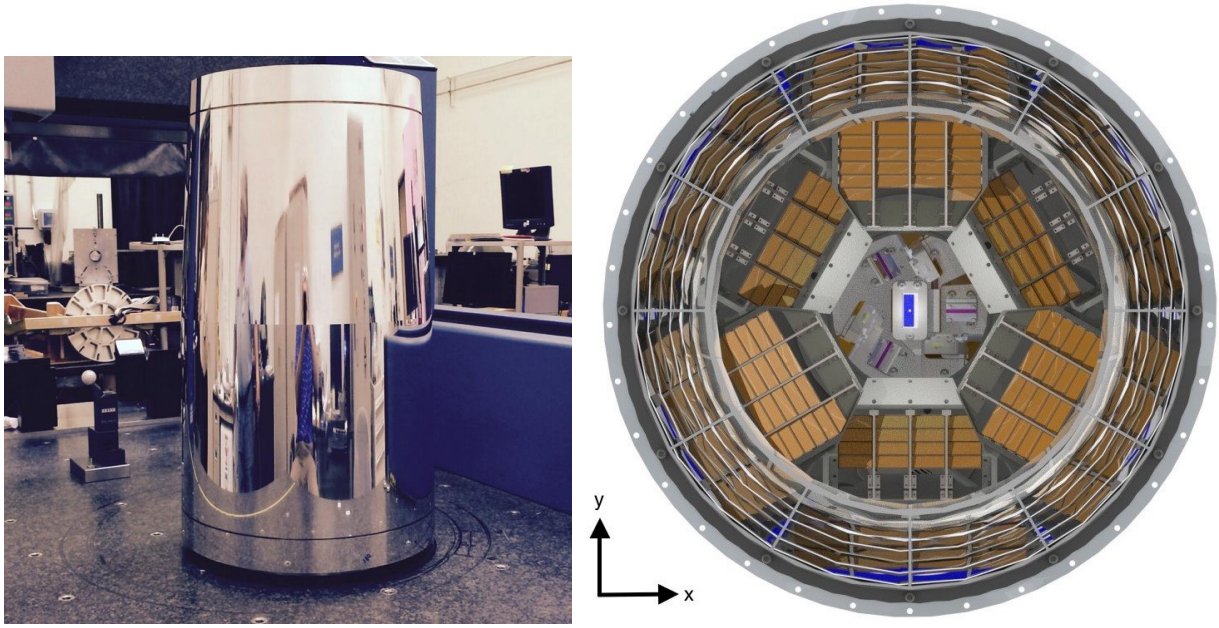

Figure 4. *Left:* A mirror mandrel made at MSFC, fabricated for the Micro-X project. The replication surface is 600 mm long. *Right:* View of the *REDSoX* Polarimeter front aperture, without the central baffling disk, vacuum box door, or focal plane baffle. Gratings are colored gold. The multilayer mirrors are magenta and the direct imaging CCD is a dark blue rectangle in the center of the focal plane; the remaining CCDs are edge-on in this view. Grating sectors with more gratings are closer to the optics. Gratings in the top and bottom sectors disperse to the right-most multilayer mirror, along the $+x$ axis.

3.2.2 Gratings

We use Critical Angle Transmission (CAT) gratings [35] developed in the Space Nanotechnology Lab (SNL) at MIT that can now be reliably produced in a 10×30 mm format [36] and up to 32×32 mm [37]. Efficiencies of 20-30% are achieved in one order (+1), as needed for the *REDSoX* Polarimeter [5, 36]. We note that the measured efficiencies in the 30-70 Å range are generally closer to the models than the measurements below 30 Å [38]. We have 5 working CAT gratings with 4 μm membrane thickness in the MIT polarimetry lab and have verified the grating efficiency at O-K (525 eV). See Heine et al. (2017) for details of our lab testing [6]. Gratings will be glued into Invar mounts designed for minimal obscuration (Egan, et al., these proceedings).

The dispersion of the grating is given by the grating equation: $m\lambda = P \sin\phi$, where P is the grating period, m is the grating order of interest (which we take to be +1) and ϕ is the dispersion angle. For the simplest grating fabrication, P is the same for all gratings in this design. Our goal is to match the dispersed wavelength to the peak reflectivity of a laterally graded multilayer (LGML), given by $\lambda = 2d\cos\theta$, where d is the multilayer period and θ is the angle of incidence relative to the LGML normal. For the LGML, $d = Gx$, where x is the distance along the LGML referenced to some location off of the LGML. Again, the simplest design is when G is the same for all LGMLs; for our prototype LGMLs, $G = 0.88$Å/mm. Defining $+x$ to be the horizontal direction to the right in Fig. 4 (right) and setting $x = 0$ to be where the 0th order lands at the plane of the LGML, then we match the LGML's Bragg peak to the grating dispersion by setting $P\sin\phi \approx Px/z = 2d\cos\theta = 2Gx\cos\theta$, giving $z = P/(2G\cos\theta)$, where z is the distance from the grating to the LGML (along the system's optical axis). See Günther et al. [2017 3] for details of the optical design, the grating placement, and system ray tracing results.

The LGML is tilted 45° to the optical axis, facing along $-y$ in Fig. 4, so gratings in the top sector ($+y$) are incident closer to graze than 45° while those in the bottom sector ($-y$) are closer to the LGML normal. Thus, the angle θ varies with the grating y position; gratings in the top sector are placed farther from the focal plane than those in the bottom sector because $\cos\theta$ is smaller when rays are closer to grazing incidence. We solved for z as a function of (x, y) for each grating [3], resulting in a stairstepped grating mount, as illustrated in Fig. 5. We have verified in a lab experiment [6] that the 10 × 30 mm CAT gratings can be curved gently as required to maintain the proper blaze condition [3].

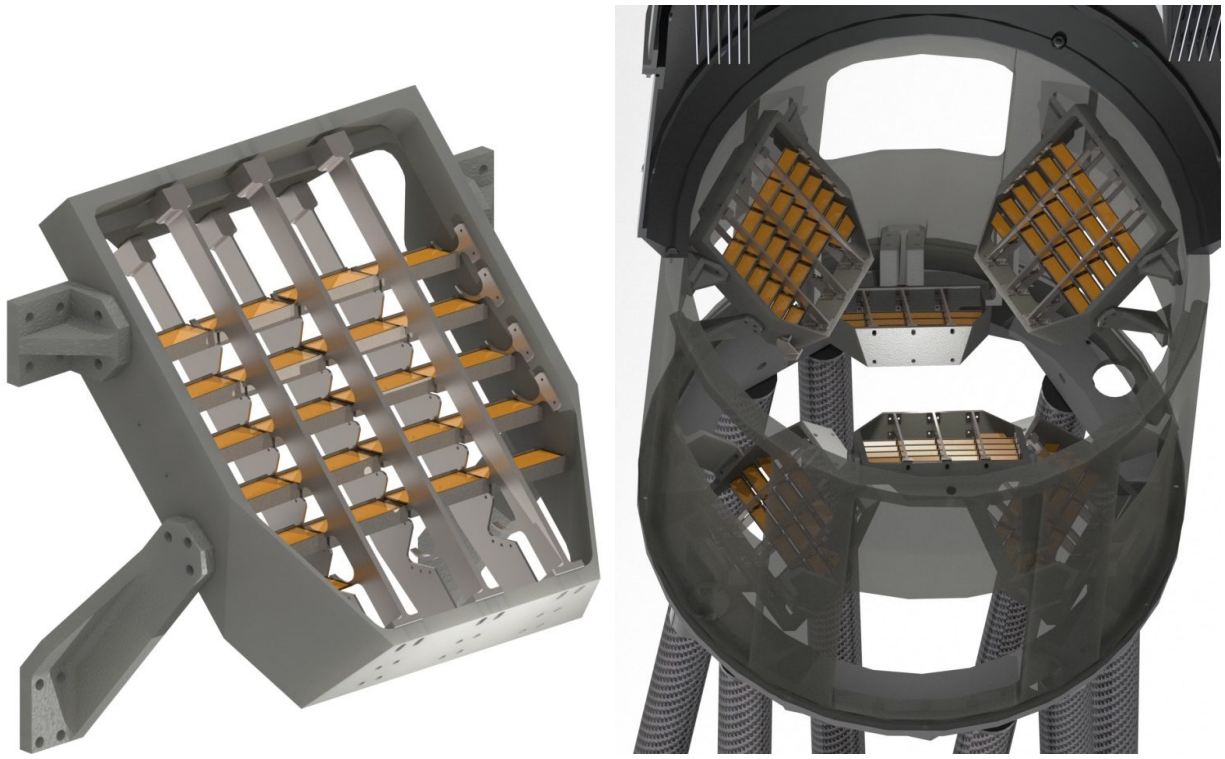

Figure 5. *Left:* Engineering design of an assembly of gratings for one sector of the *REDSoX* Polarimeter. The gratings are blazed to disperse to the right when facing the assembly. The gratings are stairstepped to match the Bragg condition at the multilayer mirror (see §3.2.2). Ribs have pins to securely position gratings below the Invar mounts and flexible arms above to maintain location. *Right:* Grating assemblies as installed on the optical bench of the *REDSoX* Polarimeter.

3.2.3 Laterally Graded Multilayer Mirrors (LGMLs)

LGMLs have been made by Reflective X-ray Optics (RXO) and the Center for X-ray Optics (CXRO) that are suitable for our design. As part of our current and previous APRA development grants, RXO fabricated 4 pairs of LGMLs on highly polished Si wafers. They all have a linear spacing variation of 0.88 Å/mm to reflect and polarize X-rays from 17Å to 73Å (170 to 730 eV). The material pairs were Cr/Sc, C/CrCo, and La/B_4C. Reflection efficiencies at 45° were measured at the Advanced Light Source (ALS) to determine the Bragg peak at 1 or 2 mm spacing for each LGML [4, 39]. Results of these tests are shown in Fig. 6, along with a picture of one LGML. Across each LGML, the Bragg peak deviates from linearity by less than 1%, $\times 2$ smaller than the FWHM of the peak.

The reflectivities of the LGMLs are critical to the performance of the *REDSoX* Polarimeter. The baseline design selects the 40-70Å wavelength range due to the the extents of the CCD detectors and the spectrometer dispersion relation. Using a precision wafer cutting facility available to us at MIT, we will cut the different LGMLs at x positions corresponding to reflectivity crossovers, as determined by measurements in the MIT Polarimetry Lab, referenced to the edge of the LGML. Our system is capable of measuring the x value using the C-K line to 10 μm [39]. We will then abut the LGMLs as we mount them onto the stands in the detector vacuum box. The LGMLs will be insulated from the LN_2-cooled mounting plate with Invar standoffs. We tested an LGML in the lab by mounting it to a LN_2-cooled plate and found no visible effects [6]. If maximally cooled, differential cooling across an LGML changes its length by less than 0.05%, or 20 μm across 40 mm, which is negligible.

3.2.4 CCD Detectors

For the CCD detectors we use commercially available CCD cameras. XCAM has recently developed a prototype system for a NASA sounding rocket experiment (Mission number 36.298) with a suitable flight electronics format. These devices are back-illuminated and used without the anti-reflection coating for an energy range of 150-2000 eV (EMCCD). These CCDs have typical quantum efficiencies of 80-90% in the energy range of 150 eV to 500 eV. The EMCCD is about 25 mm square with over 1500 pixels in both dimensions.

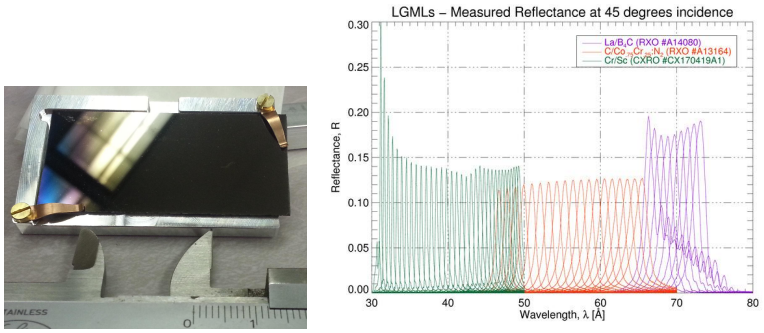

Figure 6. *Left:* A laterally graded multilayer coated mirror (LGML) from RXO in a lab holder. It is about 0.5 mm thick and 47 mm long. The multilayer period, d, increases from left to right. *Right:* Reflectivity measurements of LGMLs [4, 39] using a partially polarized beam at the ALS in Berkeley. The reflectivity was sampled at 1 mm spacing, starting below 3 nm (about 0.4 keV).

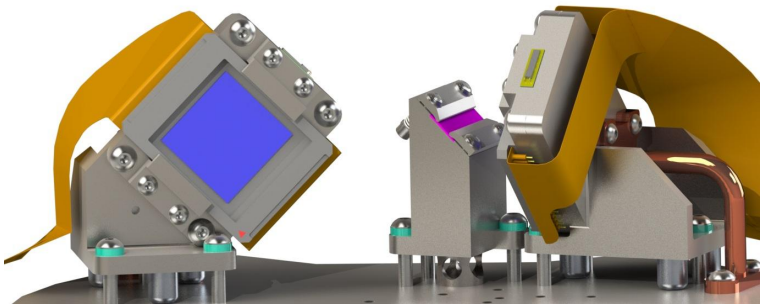

Figure 7. Design of part of the focal plane, with two CCDs (one in blue), an LGML (magenta), and flex prints (gold). Standoffs are used to keep some parts (e.g. LGMLs) from the LN_2-cooled plate onto which these parts are mounted and for better CCD thermal control. A Cu cold strap connects the CCD mount to the cooled base. Detectors are mounted diagonally to extend the spectroscopic range of the system.

The focal plane design is shown in Fig. 8. We do not expect the 3 CCDs which receive the dispersed X-rays to receive optical light from the gratings reflected by the LGMLs, so these will not have filters, giving quantum efficiencies of about 85% in the band of interest. However, baffling is needed to shield these CCDs from stray light (see Fig. 8). An imaging CCD receives the gratings' zeroth orders and needs an optical blocking filter (OBF). We plan to purchase the OBF and two spares from Luxel and mount the OBF just above the CCD surface. The filter is 50 nm Al on 200 nm polyimide film mounted in a frame supplied by Luxel.

3.3 System Considerations

Details of the engineering design can be found in a companion paper [2].

3.3.1 Attitude Control and Alignment

If pointing jitter is $\gtrsim 15''$ (3σ), light would be lost as the dispersed spectrum is displaced from the Bragg peak of the LGML along the dispersion. Therefore, we require the rocket attitude control system (ACS) to hold attitude to $\sim 5''$. Acquisition by the ACS is good to about $3'$, so the pointing direction must be adjusted so that the target lands on the aimpoint of the 0th order detector (set during system alignment) to within $5''$. We must then determine the centroid of the target to $3''$ and then request an attitude maneuver. For a mirror with an HPD of $30''$, 100 counts are required in 0th order. The expected 0th order count rate for Mk 421 is about 80 cnt/s, so we will obtain 800 counts in 10 s with some pileup in 1D if row summing. ACS settling is required after rotating the telescope 60° half-way through the observation in order to change the position angles of the LGML mirrors with respect to the sky to check for spurious systematic errors. We expect a net exposure time of about 300 s.

3.3.2 Data Handling

The count rate in each detector will be measured after selecting for the expected energy range based on the grating dispersion and using CCD resolution to reduce background. The expected number of counts in angular bin ψ_i is

$$\lambda_i = [1 + \mu(q \cos 2\psi_i + u \sin 2\psi_i)] f A T \Delta E \tag{1}$$

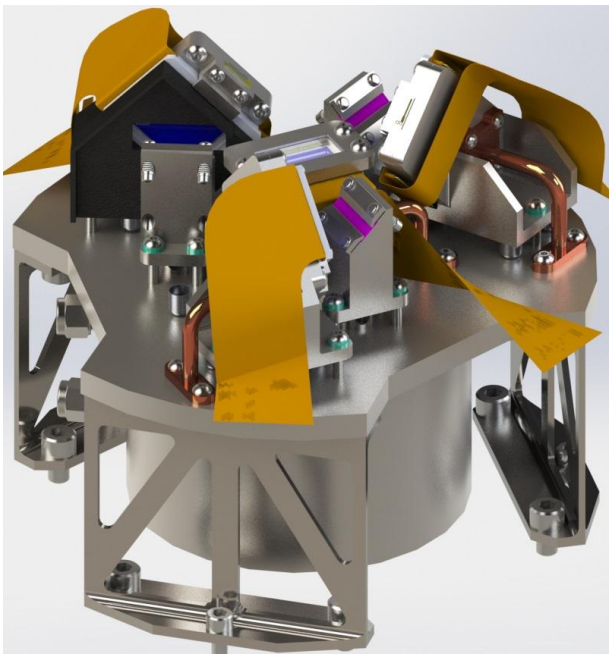

Figure 8. Interior of the detector vacuum chamber showing almost all focal plane components: LGMLs (magenta), CCD faces (blue), and flex prints (gold). A black anodized CCD baffle with a horizontal rectangular aperture restricts the view of the CCDs to its LGML.

where f is the source flux in ph/cm^2/s/keV, μ is the modulation factor at energy E, A is the system effective area, T is the exposure time, and q and u are the fractional Stokes parameters, given by $Q = \Pi \cos\phi_0 = qI$ and $U = \Pi \sin\phi_0 = uI$, respectively. The polarization fraction is then $p \equiv \Pi/I = (q^2 + u^2)^{1/2}$ and the source phase angle is $\phi_0 = \tan^{-1} u/q$. The electric vector position angle (EVPA) is $\varphi = \phi_0/2$. A likelihood analysis of the observed counts will give the estimates of f, p, and φ. The raw frames are the largest component of the data set, expected to be about one GB in total.

3.3.3 Background

From the Suzaku mission, the particle background in the backside-illuminated CCD was 5×10^{-8} cnt/s/keV/pixel, or 1.5×10^{-5} cnt/s/mm^2 in a 0.2 keV band at 0.3 keV [40]. In the cross dispersion direction, the dispersed spectra extraction region will be about twice the size of the optics HPD, about 60″, or 0.7 mm wide. In the dispersion direction, the spectra are 35 mm long. Using three detectors and exposing for 300 s yields 0.3 counts expected from particles. The X-ray background in the *REDSoX* Polarimeter bandpass is dominated by Galactic emission, about 10^{-3} cnt/s/(arcmin)^2 in the ROSAT C band, or 540 ph/cm^2/s/sr/keV for ROSAT's area (220 cm^2) and bandwidth (0.1 keV) [41]. Thus, we expect about 30 cnt in 300 s across the *REDSoX* Polarimeter band in the solid angle of each detector. The LGMLs, however, have a 2% bandpass, giving < 2 counts expected across the 3 detectors. Compared to the source, at over 1000 counts, these backgrounds are negligible. To avoid solar scattered background, we require that the sun-earth angle be $> 120°$, as demonstrated by ROSAT [41].

3.3.4 Baseline Performance

For a polarimeter, a figure of merit is the minimum detectable polarization (MDP) at 99% confidence, given as a fraction: MDP $= 4.29\sqrt{(R+B)/T}/(\mu R)$, where R is the source count rate, B is the background count rate in a region that is the size of a typical image, T is the observation time, and μ is the modulation factor of the signal relative to the average signal for a source that is 100% polarized [42]. For the most polarimeters operating in the 2-8 keV band, the modulations factors peak at $0.5-0.7$, while for the *REDSoX* Polarimeter, $\mu = 0.92-0.96$ (based on raytracing). The effective area of the system was validated using raytracing developed for the *REDSoX* Polarimeter project [3]. The raytrace accounted for grating obscuration by the linear and hexagonal supports (20% each) and realized grating efficiencies. The grasp of the system, defined as $\mathcal{G} = \int A(\lambda)d\lambda$ is 185 cm^{2}Å, giving about 5 counts/s for Mk 421. With $R \gg B$ (see § 3.3.3), **the MDP from a 300 s observation of Mk 421 will be 11%**.

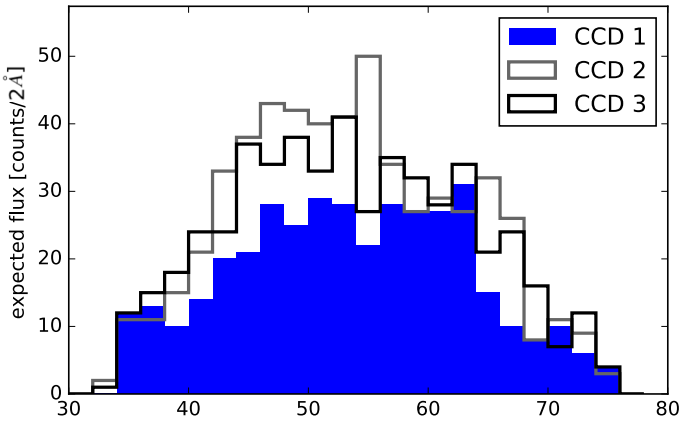

Figure 9. Sample result from raytracing an observation of Mk 421 in the simulation, the source is 20% polarized in a direction perpendicular to the mirror associated with CCD 1, which clearly shows fewer counts than either of the two remaining CCDs. If the source were randomly polarized, we would observe an average of 25 counts per 2Å bin across a 40Å band in each channel (1500 counts total), demonstrating how clearly a polarization of 20% can be detected.

4. TOWARD AN ORBITING SOFT X-RAY POLARIMETER

The *REDSoX* Polarimeter design can be extended simply to a polarimeter suitable for a Mission of Opportunity for the International Space Station, a future NASA small explorer orbiting mission, or a foreign government's X-ray mission such as eXTP, the enhanced X-ray Timing and Polarimetry mission (eXTP [43]). One of our prime goals of this project is to validate the performance of the basic design of the *REDSoX* Polarimeter. There is considerable interest in matching a soft X-ray polarimeter of our design with other polarimeters working at higher energies. For example, our design is the baseline for an X-ray Polarimetry Probe proposed recently to NASA for concept study funding. This concept would use common optics with gratings to disperse to LGMLs and CCD detectors for the soft channel (as in the *REDSoX* Polarimeter), a time projection chamber (TPC) polarimeter using the photoelectron tracking method proposed for GEMS [44] and PRAXyS [45] to detect X-rays in the 2-8 keV range, and LiH/scintillator scattering rods surrounded by Cd-Zn-Te detectors to measure up to 50 keV (based on X-Calibur, [46]). The gratings are practically transparent to X-rays above 2 keV, and the TPC can be constructed with an exit window to allow high energy X-rays to pass through to the scattering instrument. This way, all instruments can share a focussing optic with large effective area.

In 200ks, an orbiting MLPol with the same components as we propose for the *REDSoX* Polarimeter would achieve an MDP of 4% for a source at 1% as bright as Mk 421. For RX J0720−3125, the MDP would be 9% in each of 10 pulse phase bins. Spectropolarimetry with MLPol could be used to test the nature of absorption features in the atmospheres of neutron stars and examine the reflected continuum between emission lines in Sy 2 galaxies. Such an instrument would complement any high energy photoelectron-tracking polarimeter such as proposed for IXPE and eXTP.

ACKNOWLEDGMENTS

Support for this work was provided by the National Aeronautics and Space Administration through grants NNX17AE11G and NNX12AH12G and by Research Investment Grants from the MIT Kavli Institute. This work was also supported in part by NASA grants NNX17AG43G and NNX15AC43G.

References

[1] Marshall, H. L., "A soft x-ray polarimeter designed for broadband x-ray telescopes," in [*Optics for EUV, X-Ray, and Gamma-Ray Astronomy III. Edited by O'Dell, Stephen L.; Pareschi, Giovanni. Proceedings of the SPIE, Volume 6688, pp. 66880Z (2007).*], *Proc. SPIE,* **6688** (2007).

[2] Egan, M. D., Hellickson, T., and Marshall, H. L., "The optomechanical design of the REDSoX sounding rocket experiment," in [*Society of Photo-Optical Instrumentation Engineers (SPIE) Conference Series*], *Proc. SPIE,* **10397**, 103971E (2017).

[3] Günther, H. M., Egan, M. D., Heilmann, R. K., Heine, S. N. T., Hellickson, T., Frost, J., Marshall, H. L., Schulz, N. S., and Theriault-Shay, A., "REDSoX: Monte-Carlo ray-tracing for a soft X-ray spectroscopy polarimeter," in [*Society of Photo-Optical Instrumentation Engineers (SPIE) Conference Series*], *Proc. SPIE,* **10399**, 103991H (2017).

[4] Marshall, H. L., Schulz, N. S., Windt, D. L., Gullikson, E. M., Craft, M., Blake, E., and Ross, C., "The use of laterally graded multilayer mirrors for soft x-ray polarimetry," in [*Society of Photo-Optical Instrumentation Engineers (SPIE) Conference Series*], *Proc. SPIE,* **9603**, 960319 (2015).

[5] Heilmann, R. K., Bruccoleri, A. R., Kolodziejczak, J., Gaskin, J. A., O'Dell, S. L., Bhatia, R., and Schattenburg, M. L., "Critical-angle x-ray transmission grating spectrometer with extended bandpass and resolving power $>$ 10,000," in [*Society of Photo-Optical Instrumentation Engineers (SPIE) Conference Series*], *Proc. SPIE,* **9905**, 99051X (2016).

[6] Heine, S. N. T., Marshall, H. L., Heilmann, R. K., Schulz, N. S., Beeks, K., Drake, F., Gaines, D., Levey, S., Windt, D. L., and Gullikson, E. M., "Laboratory progress in soft X-ray polarimetry," in [*Society of Photo-Optical Instrumentation Engineers (SPIE) Conference Series*], *Proc. SPIE,* **10399**, 103991H (2017).

[7] Weisskopf, M. C., Ramsey, B., O'Dell, S., Tennant, A., Elsner, R., Soffitta, P., Bellazzini, R., Costa, E., Kolodziejczak, J., Kaspi, V., Muleri, F., Marshall, H., Matt, G., and Romani, R., "The Imaging X-ray Polarimetry Explorer (IXPE)," in [*Society of Photo-Optical Instrumentation Engineers (SPIE) Conference Series*], *Proc. SPIE,* **9905**, 990517 (2016).

[8] Marshall, H. L., Heilmann, R. K., Schulz, N. S., and Murphy, K. D., "Broadband soft x-ray polarimetry," in [*Society of Photo-Optical Instrumentation Engineers (SPIE) Conference Series*], *Proc. SPIE,* **7732** (2010).

[9] Ginzburg, V. L. and Syrovatskii, S. I., "Cosmic Magnetobremsstrahlung (synchrotron Radiation)," *ARA&A,* **3**, 297 (1965).

[10] Jannuzi, B. T., Smith, P. S., and Elston, R., "The optical polarization properties of X-ray-selected BL Lacertae objects," *ApJ,* **428**, 130–142 (1994).

[11] Hovatta, T., Lindfors, E., Blinov, D., Pavlidou, V., Nilsson, K., Kiehlmann, S., Angelakis, E., Fallah Ramazani, V., Liodakis, I., Myserlis, I., Panopoulou, G. V., and Pursimo, T., "Optical polarization of high-energy BL Lacertae objects," *A&A,* **596**, A78 (2016).

[12] Burn, B. J., "On the depolarization of discrete radio sources by Faraday dispersion," *MNRAS,* **133**, 67 (1966).

[13] Giroletti, M., Giovannini, G., Feretti, L., Cotton, W. D., Edwards, P. G., Lara, L., Marscher, A. P., Mattox, J. R., Piner, B. G., and Venturi, T., "Parsec-Scale Properties of Markarian 501," *ApJ,* **600**, 127–140 (2004).

[14] Marscher, A. P., "Relativistic jets and the continuum emission in QSOs," *ApJ,* **235**, 386–391 (1980).

[15] Marscher, A. P. and Gear, W. K., "Models for high-frequency radio outbursts in extragalactic sources, with application to the early 1983 millimeter-to-infrared flare of 3C 273," *ApJ,* **298**, 114–127 (1985).

[16] Gaidos, J. A., Akerlof, C. W., Biller, S., Boyle, P. J., Breslin, A. C., Buckley, J. H., Carter-Lewis, D. A., Catanese, M., Cawley, M. F., Fegan, D. J., Finley, J. P., Gordo, J. B., Hillas, A. M., Krennrich, F., Lamb, R. C., Lessard, R. W., McEnery, J. E., Masterson, C., Mohanty, G., Moriarty, P., Quinn, J., Rodgers, A. J., Rose, H. J., Samuelson, F., Schubnell, M. S., Sembroski, G. H., Srinivasan, R., Weekes, T. C., Wilson, C. L., and Zweerink, J., "Extremely rapid bursts of TeV photons from the active galaxy Markarian 421," *Nature,* **383**, 319–320 (1996).

[17] van Adelsberg, M. and Lai, D., "Atmosphere models of magnetized neutron stars: QED effects, radiation spectra and polarization signals," *MNRAS,* **373**, 1495–1522 (2006).

[18] Suleimanov, V., Hambaryan, V., Potekhin, A. Y., van Adelsberg, M., Neuhäuser, R., and Werner, K., "Radiative properties of highly magnetized isolated neutron star surfaces and approximate treatment of absorption features in their spectra," *A&A,* **522**, A111 (2010).

[19] Heyl, J. S., Shaviv, N. J., and Lloyd, D., "The high-energy polarization-limiting radius of neutron star magnetospheres - i. slowly rotating neutron stars," *Monthly Notices of the Royal Astronomical Society* **342**(1), 134–144 (2003).

[20] Heyl, J. S. and Shaviv, N. J., "QED and the high polarization of the thermal radiation from neutron stars," *PhysRevD,* **66**, 023002–+ (2002).

[21] Heyl, J. S. and Shaviv, N. J., "Polarization evolution in strong magnetic fields," *MNRAS,* **311**, 555–564 (2000).

[22] González Caniulef, D., Zane, S., Taverna, R., Turolla, R., and Wu, K., "Polarized thermal emission from X-ray dim isolated neutron stars: the case of RX J1856.5-3754," *MNRAS,* **459**, 3585–3595 (2016).

[23] Mignani, R. P., Testa, V., González Caniulef, D., Taverna, R., Turolla, R., Zane, S., and Wu, K., "Evidence for vacuum birefringence from the first optical-polarimetry measurement of the isolated neutron star RX J1856.5-3754," *MNRAS,* **465**, 492–500 (2017).

[24] Haberl, F., Zavlin, V. E., Trümper, J., and Burwitz, V., "A phase-dependent absorption line in the spectrum of the X-ray pulsar RX J0720.4-3125," *A&A,* **419**, 1077–1085 (2004).

[25] Haberl, F., "The magnificent seven: magnetic fields and surface temperature distributions," *Ap&SS,* **308**, 181–190 (2007).

[26] Kii, T., "X-ray polarizations from accreting strongly magnetized neutron stars - Case studies for the X-ray pulsars 4U 1626-67 and Hercules X-1," *PASJ,* **39**, 781–800 (1987).

[27] Markoff, S., Falcke, H., and Fender, R., "A jet model for the broadband spectrum of XTE J1118+480. Synchrotron emission from radio to X-rays in the Low/Hard spectral state," *A&A,* **372**, L25–L28 (2001).

[28] Vieyro, F. L., Romero, G. E., and Chaty, S., "Modeling the polarization of high-energy radiation from accreting black holes. A case study of XTE J1118+480," *A&A,* **587**, A63 (2016).

[29] McClintock, J. E., Haswell, C. A., Garcia, M. R., Drake, J. J., Hynes, R. I., Marshall, H. L., Muno, M. P., Chaty, S., Garnavich, P. M., Groot, P. J., Lewin, W. H. G., Mauche, C. W., Miller, J. M., Pooley, G. G., Shrader, C. R., and Vrtilek, S. D., "Complete and Simultaneous Spectral Observations of the Black Hole X-Ray Nova XTE J1118+480," *ApJ,* **555**, 477–482 (2001).

[30] McNamara, A. L., Kuncic, Z., and Wu, K., "X-ray polarization in relativistic jets," *MNRAS,* **395**, 1507–1514 (2009).

[31] Schnittman, J. D. and Krolik, J. H., "X-ray Polarization from Accreting Black Holes: The Thermal State," *ApJ,* **701**, 1175–1187 (2009).

[32] Ramsey, B. D., Elsner, R. F., Engelhaupt, D., Gubarev, M. V., Kolodziejczak, J. J., O'Dell, S. L., Speegle, C. O., and Weisskopf, M. C., "The development of hard x-ray optics at MSFC," in [*Optics for EUV, X-Ray, and Gamma-Ray Astronomy*], Citterio, O. and O'Dell, S. L., eds., *Proc. SPIE,* **5168**, 129–135 (2004).

[33] Figueroa-Feliciano, E., Adams, J. S., Baker, R., Bandler, S. R., Dewey, D., Doriese, W. B., Eckart, M. E., Hamersma, R., Hilton, G. C., Hwang, U., Irwin, K. D., Kelley, R. L., Kilbourne, C. A., Kissel, S. E., Leman, S. W., McCammon, D., Oakley, P. H. H., Okajima, T., O'Neal, R. H., Petre, R., Porter, F. S., Reintsema, C. D., Rutherford, J. M., Saab, T., Serlemitsos, P., Soong, Y., Trowbridge, S. N., and Wikus, P., "Update on the Micro-X Sounding Rocket payload," in [*Space Telescopes and Instrumentation 2012: Ultraviolet to Gamma Ray*], *Proc. SPIE,* **8443**, 84431B (2012).

[34] Cash, W., "X-ray optics - A technique for high resolution imaging," *Appl.Optics,* **26**, 2915–2920 (1987).

[35] Heilmann, R. K., Ahn, M., Bautz, M. W., Foster, R., Huenemoerder, D. P., Marshall, H. L., Mukherjee, P., Schattenburg, M. L., Schulz, N. S., and Smith, M., "Development of a critical-angle transmission grating spectrometer for the International X-Ray Observatory," in [*Optics for EUV, X-Ray, and Gamma-Ray Astronomy IV*], *Proc. SPIE,* **7437**, 74370G (2009).

[36] Heilmann, R. K., Bruccoleri, A. R., and Schattenburg, M. L., "High-efficiency blazed transmission gratings for high-resolution soft x-ray spectroscopy," in [*Society of Photo-Optical Instrumentation Engineers (SPIE) Conference Series*], *Proc. SPIE,* **9603**, 960314 (2015).

[37] Heilmann, R. K., Bruccoleri, A. R., Song, J., Kolodziejczak, J., Gaskin, J. A., O'Dell, S. L., Cheimetz, P., Hertz, E., Smith, R., Burwitz, V., Hartner, G., La Caria, M.-M., and Schattenburg, M. L., "Critical-angle transmission grating technology development for high resolving power soft x-ray spectrometers on Arcus and Lynx ," in [*Society of Photo-Optical Instrumentation Engineers (SPIE) Conference Series*], *Proc. SPIE,* **10399**, 103991H (2017).

[38] Heilmann, R. K., Ahn, M., Bruccoleri, A., Chang, C.-H., Gullikson, E. M., Mukherjee, P., and Schattenburg, M. L., "Diffraction efficiency of 200-nm-period critical-angle transmission gratings in the soft x-ray and extreme ultraviolet wavelength bands," *Appl.Optics,* **50**, 1364 (2011).

[39] Marshall, H. L., Schulz, N. S., Windt, D. L., Gullikson, E. M., Blake, E., Getty, D., and McInturff, Z., "The use of laterally graded multilayer mirrors for soft X-ray polarimetry," in [*Society of Photo-Optical Instrumentation Engineers (SPIE) Conference Series*], *Proc. SPIE,* **9144**, 1 (2014).

[40] LaMarr, B., Grant, C., Kissel, S., Prigozhin, G., Bautz, M., Tsuru, T. G., Tsunemi, H., Dotani, T., Hayashida, K., and Matsumoto, H., "Front- and back-illuminated x-ray CCD performance in low- and high-Earth orbit: performance trends of Suzaku XIS and Chandra ACIS detectors," in [*Space Telescopes and Instrumentation 2008: Ultraviolet to Gamma Ray*], *Proc. SPIE,* **7011**, 70112C (2008).

[41] Snowden, S. L., Egger, R., Freyberg, M. J., McCammon, D., Plucinsky, P. P., Sanders, W. T., Schmitt, J. H. M. M., Trümper, J., and Voges, W., "ROSAT Survey Diffuse X-Ray Background Maps. II.," *ApJ,* **485**, 125–135 (1997).

[42] Weisskopf, M. C., Elsner, R. F., Kaspi, V. M., O'Dell, S. L., Pavlov, G. G., and Ramsey, B. D., "X-Ray Polarimetry and Its Potential Use for Understanding Neutron Stars," in [*Astrophysics and Space Science Library*], Becker, W., ed., *Astrophysics and Space Science Library* **357**, 589 (2009).

[43] Zhang, S. N., Feroci, M., Santangelo, A., Dong, Y. W., Feng, H., Lu, F. J., Nandra, K., Wang, Z. S., Zhang, S., Bozzo, E., Brandt, S., De Rosa, A., Gou, L. J., Hernanz, M., van der Klis, M., Li, X. D., Liu, Y., Orleanski, P., Pareschi, G., Pohl, M., Poutanen, J., Qu, J. L., Schanne, S., Stella, L., Uttley, P., Watts, A., Xu, R. X., Yu, W. F., in 't Zand, J. J. M., Zane, S., Alvarez, L., Amati, L., Baldini, L., Bambi, C., Basso, S., Bhattacharyya S., , R., B., Belloni, T., Bellutti, P., Bianchi, S., Brez, A., Bursa, M., Burwitz, V., Budtz-Jørgensen, C., Caiazzo, I., Campana, R., Cao, X., Casella, P., Chen, C. Y., Chen, L., Chen, T., Chen, Y., Chen, Y., Chen, Y. P., Civitani, M., Coti Zelati, F., Cui, W., Cui, W. W., Dai, Z. G., Del Monte, E., de Martino, D., Di Cosimo, S., Diebold, S., Dovciak, M., Donnarumma, I., Doroshenko, V., Esposito, P., Evangelista, Y., Favre, Y., Friedrich, P., Fuschino, F., Galvez, J. L., Gao, Z. L., Ge, M. Y., Gevin, O., Goetz, D., Han, D. W., Heyl, J., Horak, J., Hu, W., Huang, F., Huang, Q. S., Hudec, R., Huppenkothen, D., Israel, G. L., Ingram, A., Karas, V., Karelin, D., Jenke, P. A., Ji, L., Korpela, S., Kunneriath, D., Labanti, C., Li, G., Li, X., Li, Z. S., Liang, E. W., Limousin, O., Lin, L., Ling, Z. X., Liu, H. B., Liu, H. W., Liu, Z., Lu, B., Lund, N., Lai, D., Luo, B., Luo, T., Ma, B., Mahmoodifar, S., Marisaldi, M., Martindale, A., Meidinger, N., Men, Y., Michalska, M., Mignani, R., Minuti, M., Motta, S., Muleri, F., Neilsen, J., Orlandini, M., Pan, A. T., Patruno, A., Perinati, E., Picciotto, A., Piemonte, C., Pinchera, M., Rachevski A., Rapisarda, M., Rea, N., Rossi, E. M. R., Rubini, A., Sala, G., Shu, X. W., Sgro, C., Shen, Z. X., Soffitta, P., Song, L., Spandre, G., Stratta, G., Strohmayer, T. E., Sun, L., Svoboda, J., Tagliaferri, G., Tenzer, G., Hong, T., Taverna, R., Torok, G., Turolla, R., Vacchi, S., Wang, J., Walton, D., Wang, K., Wang, J. F.,

Wang, R. J., Wang, Y. F., Weng, S. S., Wilms, J., Winter, B., Wu, X., Wu, X. F., Xiong, S. L., Xu, Y. P., Xue, Y. Q., Yan, Z., Yang, S., Yang, X., Yang, Y. J., Yuan, F., Yuan, W. M., Yuan, Y. F., Zampa, G., Zampa, N., Zdziarski, A., Zhang, C., Zhang, C. L., Zhang, L., Zhang, X., Zhang, Z., Zhang, W. D., Zheng, S. J., Zhou, P., and Zhou X. L., "eXTP: Enhanced X-ray Timing and Polarization mission," in [*Society of Photo-Optical Instrumentation Engineers (SPIE) Conference Series*], *Proc. SPIE,* **9905**, 99051Q (2016).

[44] Swank, J. and the GEMS team, "Gravity and Extreme Magnetism SMEX (GEMS)," in [*X-ray Polarimetry: A New Window in Astrophysics by Ronaldo Bellazzini*], Bellazzini, R., Costa, E., Matt, G., and Tagliaferri, G., eds., 251 (2010).

[45] Jahoda, K., Kallman, T. R., Kouveliotou, C., Angelini, L., Black, J. K., Hill, J. E., Jaeger, T., Kaaret, P. E., Markwardt, C. B., Okajima, T., Petre, R., Schnittman, J., Soong, Y., Strohmayer, T. E., Tamagawa, T., and Tawara, Y., "The Polarimeter for Relativistic Astrophysical X-ray Sources," in [*Society of Photo-Optical Instrumentation Engineers (SPIE) Conference Series*], *Proc. SPIE,* **9905**, 990516 (2016).

[46] Beilicke, M., Kislat, F., Zajczyk, A., Guo, Q., Endsley, R., Stork, M., Cowsik, R., Dowkontt, P., Barthelmy, S., Hams, T., Okajima, T., Sasaki, M., Zeiger, B., de Geronimo, G., Baring, M. G., and Krawczynski, H., "Design and Performance of the X-ray Polarimeter X-Calibur," *Journal of Astronomical Instrumentation* **3**, 1440008 (2014).